Particle Accelerators, Vol. 59, pp. 1–17
Reprints available directly from the publisher
Photocopying permitted by license only

FREQUENCY TUNABILITY AND PHASE STABILITY OF GYROKLYSTRON AMPLIFIERS FOR DRIVING LINEAR ACCELERATORS

GIRISH P. SARAPH *

Institute for Plasma Research, University of Maryland, College Park, MD 20742-3511, USA

(Received 5 March 1997; In final form 14 August 1997)

High power, pulsed, relativistic gyroklystron amplifiers are being developed for driving future linear colliders. Detailed analysis is performed to determine frequency tunability and phase stability of these devices. Nonlinear, time-dependent simulations are carried out using two designs of X and Ku band gyroklystrons operating at the fundamental and second harmonic frequencies, respectively. It is shown that the X band design is rather insensitive to the variation in cold cavity frequency of the output cavity. Whereas, the Ku band design is very sensitive and has a narrow bandwidth corresponding to efficient operation. However, significant degree of frequency tunability can be achieved by making small changes in the magnetic field amplitude. Studies of time variations of efficiency and output phase under a typical beam voltage pulse are presented. It is shown that the shape of the pulse and its noise level play important roles in determining the phase stability of the device.

Keywords: Electron beam devices; Gyroklystrons; Power supplies; Radio-frequency devices; RF sources

I. INTRODUCTION

Efficient, 100 MW RF sources in the X and Ku frequency bands with pulse-lengths of 1 μs are being developed for future electron–positron colliders with proposed center of mass energies of 1 TeV and more.[1] The relativistic gyroklystron is one of the prime candidates being

* E-mail: girish@eng.umd.edu.

considered to fulfill these requirements.[2] Early gyroklystron experiments at Maryland have achieved 27–32 MW power levels and about 30% efficiency in the X and K bands.[3–5] The current experiments are based on the 100–150 MW designs in X and Ku bands with over 40% efficiencies.[6] The efficiency level can be increased above 50% level by using a single-stage depressed collector for energy recovery from the spent beam.[7] In addition to the power and efficiency requirements, gyroklystrons should also meet the synchronization criteria to be suitable for driving large accelerators. Hundreds of these devices would have to be synchronized in frequency and output phases. This paper deals with the synchronization study of relativistic gyroklystron amplifiers.

One of the issues important for synchronization is to account for manufacturing tolerances which may cause spread in the cold cavity frequencies of gyroklystron cavities about their design values. Typically, 1 mil (1/1000 inch) tolerance in radial dimensions could lead to 10–20 MHz changes in the cold cavity frequency of the X and Ku band cavities. If the design is very sensitive to this frequency then it would lead to degradation in its efficiency. Thus, it is desirable to have some degree of tunability with respect to the cold cavity frequency to achieve frequency synchronization without sacrificing device efficiency.

Another important issue is phase stability of the output radiation. The output phase depends on the gyrophase of the bunched electron beam at the entrance of the output cavity which in turn depends on the particle velocities through the drift section. Thus, the output phase is very sensitive to the beam voltage. The shape of the voltage pulse and its noise level play a crucial role in determining the phase stability of the device.

We analyzed these synchronization issues by considering two specific designs of two-cavity, coaxial gyroklystron amplifiers operating in the X and Ku bands. Details of these designs are presented in[6] and the operating parameters are tabulated in Table I. We refer to the two designs as 1-1 and 1-2 systems, respectively, based on the specific cyclotron harmonics in each cavity. A schematic diagram of the interaction region of a two-cavity, coaxial gyroklystron system is shown in Figure 1. Simulations take into account the velocity spread in the beam at the entrance of the interaction region.

A nonlinear, time-dependent code is used to study frequency tunability and phase stability of gyroklystrons. A brief description of the

TABLE I Operating parameters of the X and Ku band gyroklystron designs

Parameters	*X band* 1-1 *design*	*Ku band* 1-2 *design*
Beam voltage (V_b)	500 kV	500 kV
Beam current (I_b)	480 A	700 A
Pitch-angle (α_0)	1.508	1.508
Avg. magnetic field (B_0)	5.0 kG	4.9 kG
Input frequency	8.568 GHz	8.568 GHz
Output frequency	8.568 GHz	17.136 GHz
Input cavity Q	50	50
Output cavity Q	122	320
Gain	21 dB	26 dB
Efficiency	39.4%	30.2%
Output power	94.6 MW	105.7 MW

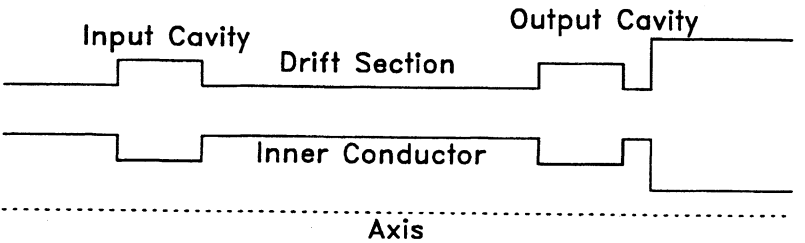

FIGURE 1 Schematic diagram of an interaction region of a two-cavity, coaxial gyroklystron system.

theoretical model is presented in Section II. Sensitivity studies with respect to the cold cavity frequency and frequency tunability results are presented in Section III. Effect of the voltage pulse and phase stability results are presented in Section IV. A summary of results and conclusions are presented in Section V.

II. THEORETICAL MODEL

The theoretical model consists of a scattering matrix formulation for determining cold-cavity fields and a nonlinear, time-dependent model for beam–wave interaction. The scattering matrix code is used to determine the cold-cavity field pattern, resonance frequency (ω_c), and quality factor (Q-value) for each cavity.[8,9] The initial X and Ku band designs[6] were modeled using a stationary, nonlinear gyroklystron code.[10] The operating parameters were optimized to get maximum

efficiency and gain. The results presented here are based on the time-dependent analysis. The original nonlinear gyroklystron code is modified to include a partial derivative of the electromagnetic field amplitude with respect to time.[11]

We use a two time-scale model in which the mode amplitudes evolve at a slow time-scale (Q/ω) and the particle motion is at a relatively fast time-scale.[12–16] However, we do not use gyro-averaging for particle motion due to a relativistic beam and short interaction cavities. The equation of evolution of the overall field amplitude a and phase ϕ for each cavity is given by

$$\left(\frac{\partial}{\partial\tau}+\frac{1}{2}+\mathrm{i}\Delta_\omega\right)a\mathrm{e}^{\mathrm{i}\phi}=-\frac{Q}{2\omega W_{\mathrm{EM}}}\int \mathrm{d}^3x\int_0^T\frac{\mathrm{d}t}{T}\vec{J}\cdot\vec{E}_{\mathrm{c}}^{\,*}\mathrm{e}^{\mathrm{i}\omega t}, \qquad (1)$$

where $\vec{J}$ is the beam current density, $\tau=\omega t/Q$ is the slow time-scale, ω is the frequency at which the cavity oscillates, $T=2\pi/\omega$ is the oscillation period, and Δ_ω is the normalized frequency shift which corresponds to the detuning between the operating frequency (which is at a harmonic multiple of the signal frequency) and the cold-cavity frequency and is given by

$$\Delta_\omega=Q\frac{\mathrm{Re}\{\omega_{\mathrm{c}}\}-\omega}{\omega}.$$

The mismatch between the operating frequency and the cold-cavity frequency includes the frequency pulling effect due to the beam–wave interaction. The design value of Δ_ω is set so as to achieve the most efficient operation. The hot-cavity electric and magnetic fields, $\vec{E}(\vec{x},t)$ and $\vec{B}(\vec{x},t)$, are given in terms of cold-cavity fields, $\vec{E}_{\mathrm{c}}(\vec{x},t)$ and $\vec{B}_{\mathrm{c}}(\vec{x},t)$, as follows:

$$\vec{E}=\mathrm{Re}\{a\mathrm{e}^{\mathrm{i}\phi}\vec{E}_{\mathrm{c}}\mathrm{e}^{-\mathrm{i}\omega t}\},$$

$$\vec{B}=\mathrm{Re}\left\{a\mathrm{e}^{\mathrm{i}\phi}\frac{\omega_{\mathrm{c}}}{\omega}\vec{B}_{\mathrm{c}}\mathrm{e}^{-\mathrm{i}\omega t}\right\}.$$

The field energy W_{EM} is defined as

$$W_{\mathrm{EM}}=\frac{1}{8\pi}\int \mathrm{d}^3x\,\vec{E}_{\mathrm{c}}\cdot\vec{E}_{\mathrm{c}}^{\,*}.$$

The equation of particle motion is expressed in the non-gyro-averaged form at a fast time-scale and is written as

$$\frac{d\vec{p}}{dt} = q[\vec{E} + \vec{\beta} \times (\vec{B} + \vec{B}_0)], \tag{2}$$

where $\vec{p}$ is the particle momentum, $\vec{\beta} = \vec{v}/c$ is the particle velocity normalized to the speed of light, and $\vec{B}_0$ is the external magnetic field which is assumed to vary adiabatically along the axial distance. The effect of AC and DC space-charge fields is neglected.[10] Equations (1) and (2) constitute a complete set of equations for the nonlinear, time-dependent model. The equations are integrated numerically by transforming them into guiding center variables and neglecting the guiding center drift due to electromagnetic fields. A detailed analysis of this method is presented in.[10] The axial velocity spread in the beam at the entrance of the interaction region is estimated to be 6.4% using the EGUN code.[17] This spread is introduced as an initial distribution of particle velocities in the nonlinear simulations.

III. FREQUENCY TUNABILITY

Typically, 1 mil (1/1000 inch) manufacturing tolerance in the radial dimension of the X and Ku band cavities could lead to 10–20 MHz changes in the cold-cavity frequency. (Our experimental pieces are manufactured to tolerances of ≤ 0.3 mil. However, the net effect due to these errors could be cumulative.) In order to achieve efficient operation at a fixed output frequency the operation of the device should not be sensitive to these changes. Otherwise some sort of frequency tunability should be introduced to compensate for these changes.

First, we determine the sensitivity of both (the X and Ku band) designs with respect to the changes in the cold-cavity frequency. It is assumed that the input cavity, which is dielectrically loaded to lower its Q value, can be tuned to the exact operating frequency. Whereas, the resonance frequency of the output cavity is determined by the cold-cavity fields. Hence, the sensitivity analysis is carried out with respect to the cold-cavity frequency of the output cavity for each design. The dependence of operating efficiency of the X band design on the cold cavity frequency is plotted in Figure 2(a). Note that the cold-cavity

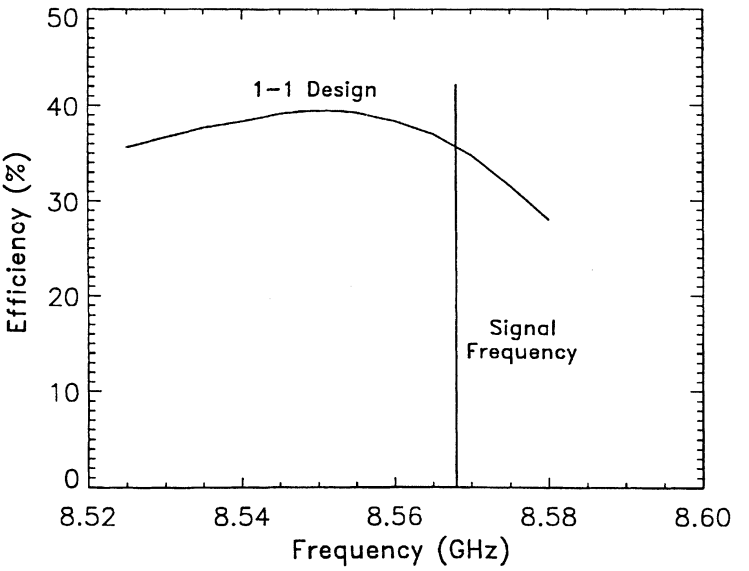

FIGURE 2(a)

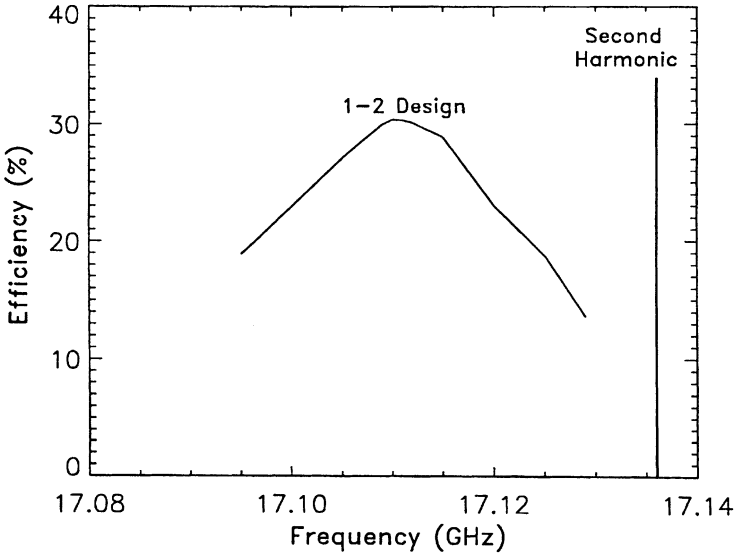

FIGURE 2(b)

FIGURE 2 Variation of efficiency versus the cold cavity frequency of the output cavity for (a) the 1-1 design (b) the 1-2 design.

frequency corresponding to the most efficient operation is about 16 MHz lower than the operating frequency of 8.568 GHz due to the frequency pulling effect. The figure shows that the design has a very broad bandwidth for high efficiency operation. A 3% drop in efficiency corresponds to about 40 MHz bandwidth which is much larger than the anticipated offset values due to manufacturing tolerances. It implies that frequency tunability is not necessary for this design.

However, the second harmonic design operating in the Ku band is very sensitive to the variation in cold-cavity frequency as shown in Figure 2(b). It should be noted that the spectrum shown in Figure 2(b) does not correspond to the instantaneous bandwidth of the device which is important for the pulse compression. The figure only shows the sensitivity of the efficiency to the cold-cavity frequency of the output cavity. A 3% drop in efficiency from its maximum value corresponds to a bandwidth of about 7 MHz only. Some sort of frequency tunability is necessary to compensate for any changes in the cold-cavity frequency from its design value due to manufacturing tolerances. Again note that the design value is about 15 MHz lower than the operating frequency which is at the second harmonic of the incident signal frequency (8.568 GHz). One possible option to achieve tunability is to use a mechanically movable part such as a plunger in the output cavity, but it may not be suitable due to high field values, perturbation of field symmetry, or complexity of designs.

Another technique to achieve frequency tunability is by varying the strength of the axial magnetic field. The optimum axial profile of the magnetic field is kept the same. However, the amplitude of the field is changed by 1% or 2% to get the required tunability. The variation of efficiency versus the cold cavity frequency for a small change in the magnetic field strength, ΔB, is shown in Figure 3 for different values of ΔB. It shows that the high efficiency operating regime can be moved to higher or lower values of cold-cavity frequency by decreasing or increasing the magnetic field strength, respectively. The cold-cavity frequency corresponding to the operating point with maximum efficiency varies linearly with ΔB as shown in Figure 4(a). The slope of the line passing through these points is about 3.8 MHz/% in ΔB or 79 MHz/kG. However, the maximum efficiency drops significantly for any changes in magnetic field strength beyond 3% as shown in Figure 4(b). The results are found to be symmetric for the positive and negative values of

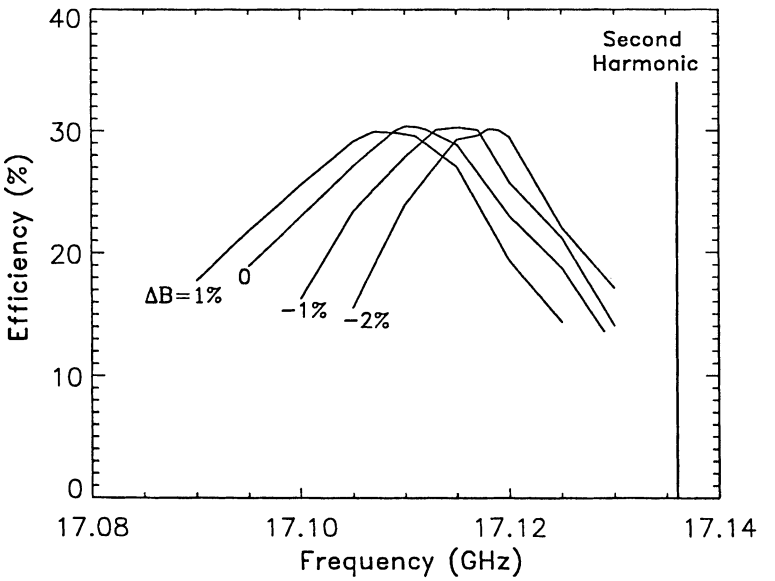

FIGURE 3 Variation of efficiency of the 1-2 design versus the cold cavity frequency of the output cavity for different values of small changes ($\Delta B = -2, -1, 0, 1\%$) in the axial magnetic field amplitude from the optimized field profile.

ΔB. Thus a limited bandwidth of about 25 MHz can be obtained by using this technique which is sufficient to compensate for any error due to manufacturing tolerances. The variation of output phase versus the cold-cavity frequency is also almost linear as shown in Figure 5 for different values of ΔB.

IV. PHASE STABILITY

Another important synchronization criterion is phase stability of the output radiation. The output phase depends on the gyrophase of the bunched electron beam at the entrance of the output cavity which in turn depends on the particle velocities through the drift section. Early gyroklystron experiments (at lower power levels) have demonstrated that the output phase is very sensitive to the beam voltage.[18,19] We have carried out time-dependent analysis for the Ku band design under the application of the voltage pulse including the rise time, the flat-top

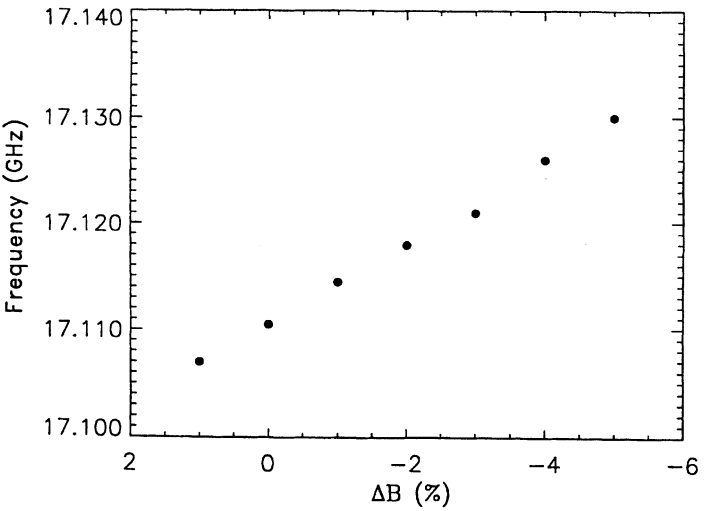

FIGURE 4(a)

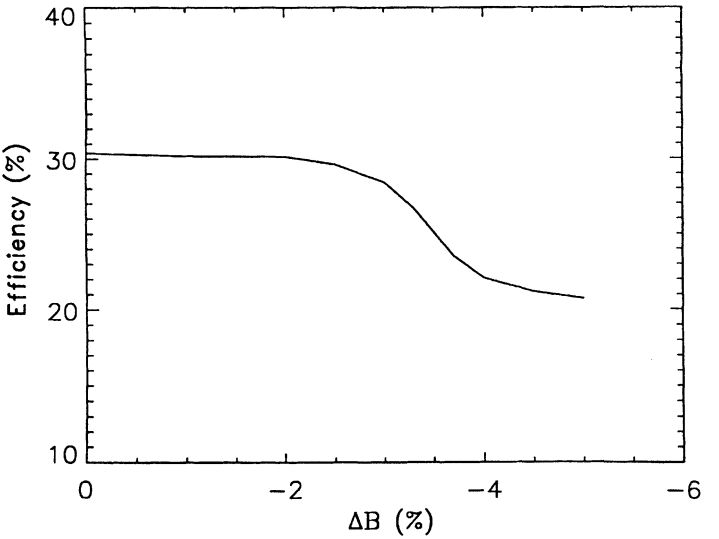

FIGURE 4(b)

FIGURE 4 Variations of (a) the optimum cold cavity frequency in the 1-2 design (corresponding to the maximum efficiency operation) and (b) the maximum efficiency at the optimized cold cavity frequency, versus small changes, ΔB, in the axial magnetic field.

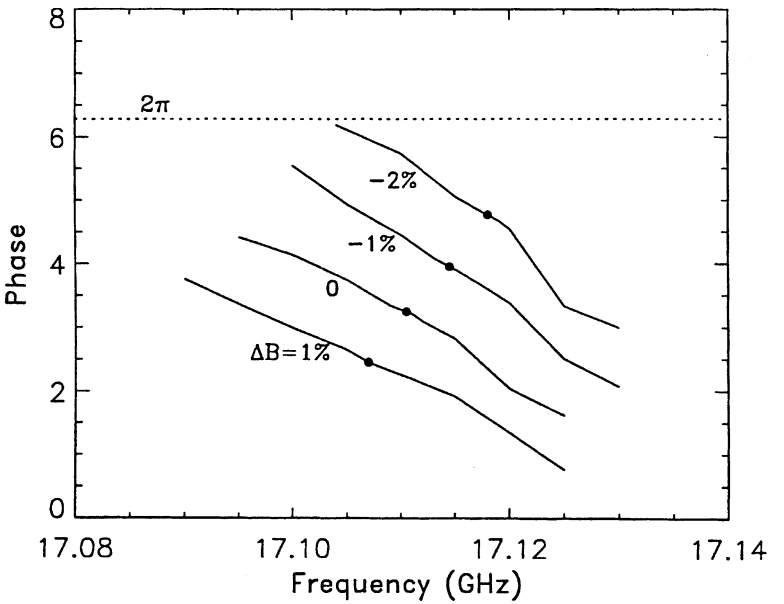

FIGURE 5 Variation of the output phase in the 1-2 design versus the cold cavity frequency of the output cavity for different values of small changes in the axial magnetic field ($\Delta B = -2, -1, 0, 1\%$). The filled circles correspond to optimum operating points (with maximum efficiency) at each value of ΔB.

portion, and the fall time. In order to determine the effect of the voltage pulse on the efficiency and output phase we have modified the nonlinear code. We use a simple model of exponentially saturating beam energy presented in.[15,16]

$$\gamma(\tau) = 1 + (\gamma_0 - 1)(1 - e^{-\tau/\tau^*}), \tag{3}$$

where τ^* is the rise time constant (t_r) of the voltage normalized to the slow time-scale and γ_0 is beam energy at the entrance of the interaction region corresponding to the flat-top or saturation period of the voltage pulse. The beam current is held constant at the operating value. We further assume that the perpendicular momentum of the electrons follows the same time dependence as the beam energy. This corresponds to the case where the voltages on all electrodes rise at the same rate and based on adiabatic relations. Thus, the average values of the perpendicular and parallel momenta of the particles ($\gamma v_\perp$ and $\gamma v_\parallel$,

respectively) at the entrance of the interaction region can be expressed as[15,16]

$$\gamma v_{\perp}(\tau) = \gamma_0 v_{\perp 0}(1 - e^{-\tau/\tau^*}),$$

$$\gamma v_{\parallel}(\tau) = \gamma_0 v_{\parallel 0}(\gamma v_{\perp}(\tau))^{1/2}(1 + \alpha_0^2 e^{-\tau/\tau^*})^{1/2},$$

where $v_{\perp 0}$, $v_{\parallel 0}$, and α_0 are the average perpendicular and parallel velocities, and pitch angle at the entrance of the interaction region corresponding to the flat-top portion of the voltage pulse. In order to simulate the falling edge at the end of the pulse we use symmetrically opposite values from the half point of the pulse-length.

We have assumed 100 ns rise time constant, about 1 μs flat-top, and a symmetric type fall for the voltage pulse. The total duration of the pulse is about 1.5 μs. The voltage pulse is shown in Figure 6(a). We have used this pulse to analyze its effect on the efficiency and phase of the second harmonic Ku band design. The variation of the normalized field amplitude in the output cavity versus time is shown in Figure 6(b). It shows that the field value has a flat-top of about 800 ns at which approximately constant output power can be delivered. The efficiency variation shown in Figure 6(c) closely matches the field amplitude variation. The output phase, however, has a rather narrow flat-top region as shown in Figure 6(d). Thus, the phase saturates much more slowly to its flat-top value as compared to the field amplitude. In order to achieve phase stability of 0.1 rad (or about 6°) only about a 300 ns portion of the pulse can be used. Better results are obtained if an absolutely constant value of the flat-top voltage is used rather than the exponential saturation described by Eq. (3). It is also possible that a small overshoot (of about 2%) at the beginning of the flat-top could hasten the phase saturation process and increase the timespan of the flat portion. Thus, an accurate shape of the voltage pulse is necessary to determine the phase stability characteristics of the device. Since this phase variation is systematic, a pre-programmed phase variation on the gyroklystron drive could in principle counteract this effect. It is advantageous to have a faster voltage rise or a smaller τ^* to get maximum flat-top period. Since $\tau^* \sim RC = (V_b/I_b)C_{eff}$, the effective capacitance C_{eff} associated with the power supply circuit and the electron gun

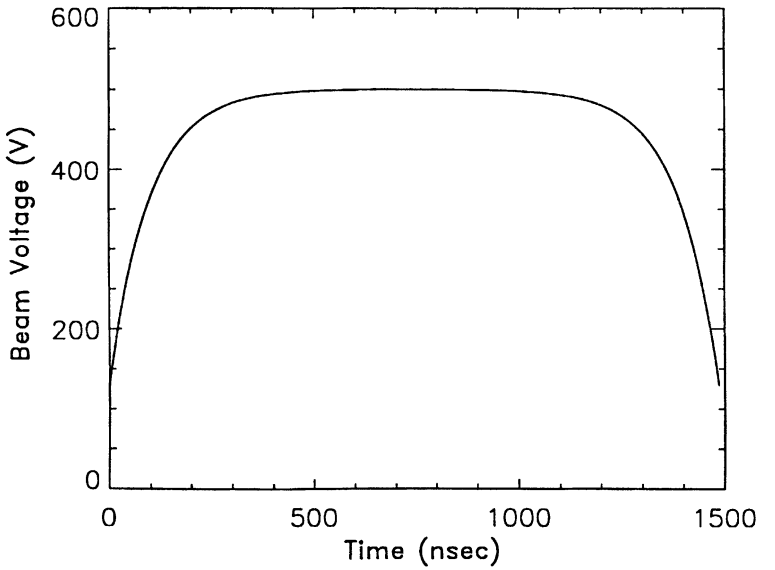

FIGURE 6(a)

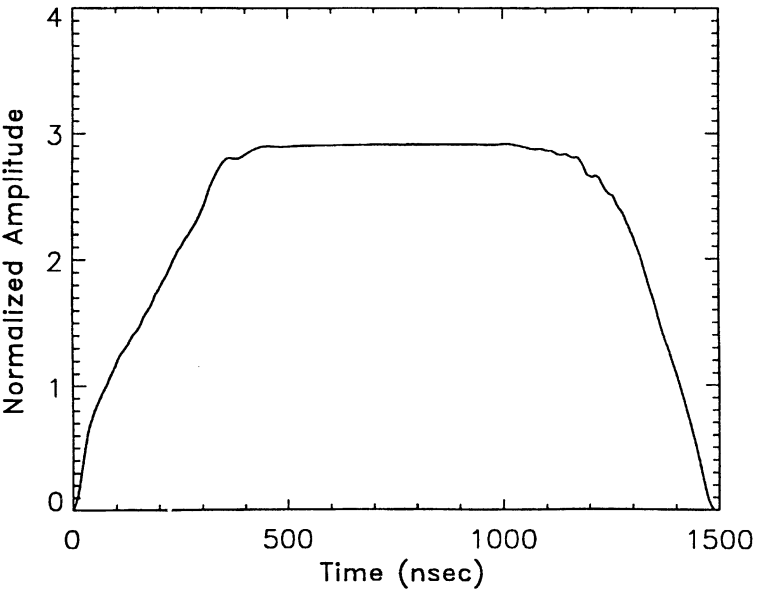

FIGURE 6(b)

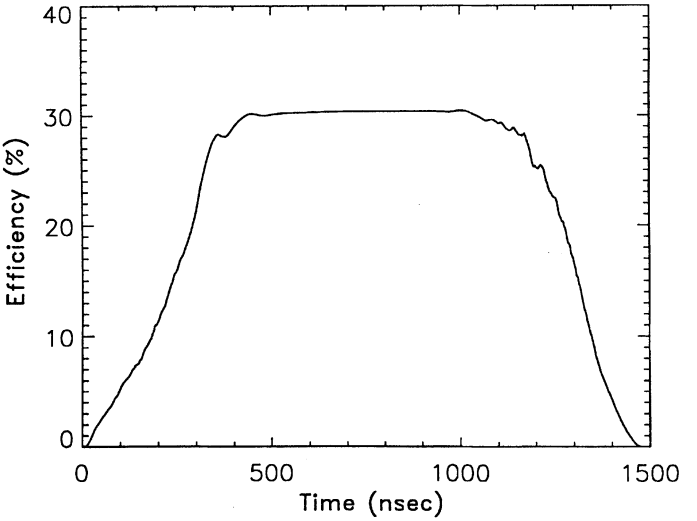

FIGURE 6(c)

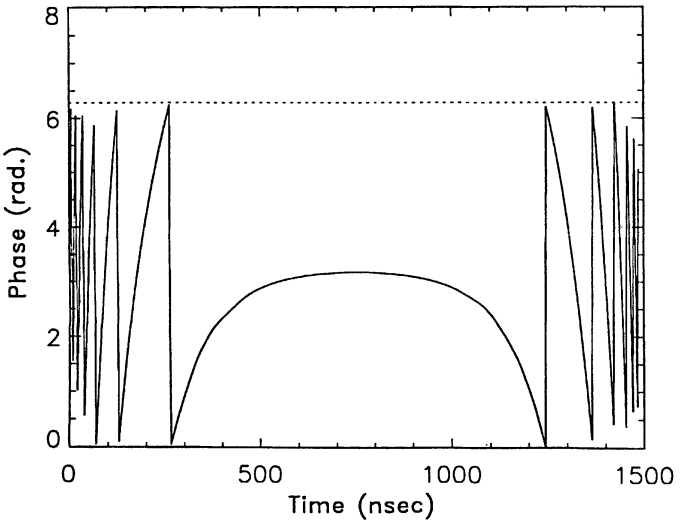

FIGURE 6(d)

FIGURE 6 Time variations of (a) the beam voltage, (b) the normalized field amplitude in the output cavity, (c) the efficiency, and (d) the output phase for the 1-2 design under the application of a given voltage pulse having 100 ns rise time constant and about 1.0 μs flat-top.

geometry should be reduced. An energy recovery system using a single-stage depressed collector and a double-anode MIG is designed in[7] which can have a faster switching time.

During the actual voltage pulse there are random fluctuations in voltage level even at the flat-top portion due to noise. We estimate the effect of noise by adding a small perturbation to the original voltage pulse. This perturbation has a half-sine form with 30 ns duration which is long as compared to the slow time-scale ($Q/\omega = 3$ ns). The perturbation is introduced after 600 ns from the start of the pulse and has an amplitude of 1% or 5 kV at the peak. The results of the time-dependent analysis with the perturbed voltage pulse are shown in Figures 7(a)–(c). Time variations of the field amplitude (shown in Figure 7(a)) and efficiency (shown in Figure 7(b)) show relatively small changes from their unperturbed variations. A 1% perturbation in voltage leads to a change of about 1% in the efficiency of the device. However, the output phase (shown in Figure 7(c)) shows a significant change (of about 0.6 rad or 34°) due to this perturbation. This implies that this design has a phase pushing factor of 6.8°/kV. However, when expressed as a percentage (34°/% voltage) it is comparable with other experimental measurements.[20] Thus, in order to achieve phase stability of 0.1 rad (required for the accelerator applications) the slow time-scale noise

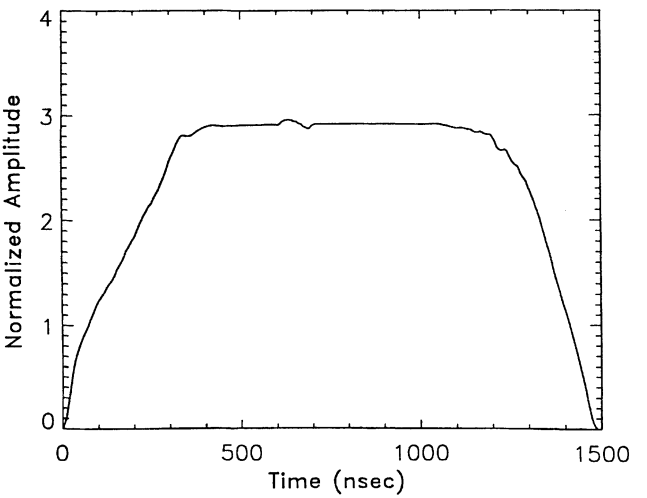

FIGURE 7(a)

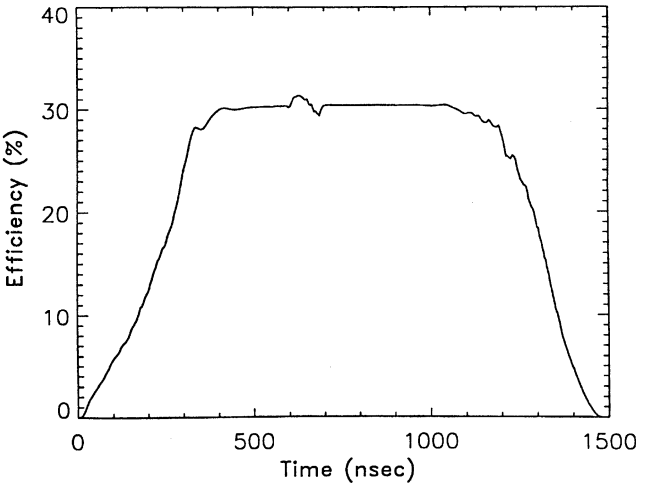

FIGURE 7(b)

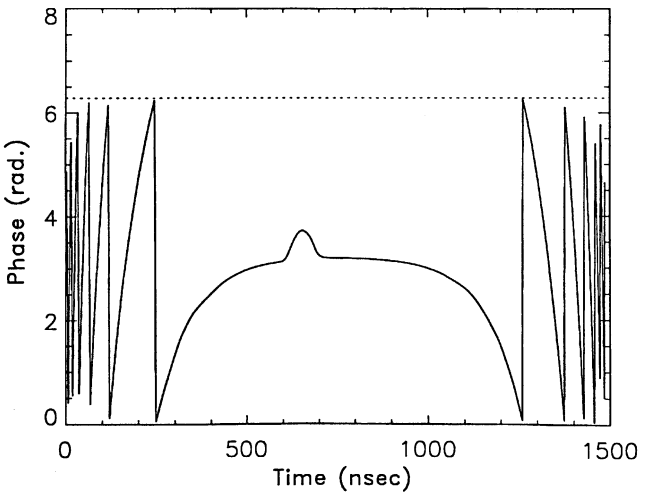

FIGURE 7(c)

FIGURE 7 Time variations of (a) the normalized field amplitude in the output cavity, (b) the efficiency, and (c) the output phase for the 1-2 design under the application of the modified voltage pulse with 1% perturbation at 600 ns from the start.

level in the beam voltage should be less than 0.2% or less than 1 kV. This is a rather stringent requirement on the voltage supply. A possible alternative is to use an external feedback loop to improve the phase stability of the device.

The analysis presented here only deals with voltage noise on the slow time-scale. The amplitude and phase of the electromagnetic field would not respond to any noise in the beam voltage which is faster than the Q/ω time-scale. This noise can be approximated by an additional velocity spread in the electron beam. Thus, the fast noise would lead to degradation in efficiency and increase in radiation linewidth,[21] but would not affect the phase stability.

V. CONCLUSIONS

We have presented a detailed study of the frequency tunability and phase stability characteristics of relativistic gyroklystron amplifiers using nonlinear, time-dependent simulations. Simulations are carried out for the two cavity, coaxial designs of fundamental and second harmonic gyroklystrons operating in the X and Ku bands, respectively.

The X band (1-1 type) design is rather insensitive to the variation in the cold cavity frequency of the output cavity. Whereas, the Ku band (1-2 type) design is very sensitive and small changes of 10–20 MHz in cold-cavity frequency due to manufacturing tolerances can lead to a significant degradation in efficiency and power levels. However, it is shown that small changes in the axial magnetic field level can compensate for the difference in the actual cold cavity frequency from its design value. Thus, a limited degree of frequency tunability can be achieved.

We have studied the effect of voltage pulse on the efficiency and output phase of the Ku band design. The simulation results show that the output phase saturates to its flat-top value much slowly as compared to the field amplitude or efficiency. A shape of the pulse and the constancy of the flat-top voltage play an important role in determining the phase stability of the device. A 1% perturbation (on the slow time-scale) in the beam voltage leads to a change of about 1% in the efficiency of the device. However, the same perturbation leads to a change of 0.6 rad in the output phase. Thus, phase stability puts a very

stringent requirement on the constancy of the flat-top voltage unless some feedback system is incorporated.

Acknowledgments

This work was supported by the U.S. Department of Energy.

The author wishes to thank Drs. Baruch Levush and Peter Latham for converting the nonlinear code for gyroklystron amplifiers into the time-dependent form. The author also acknowledges the help by Dr. Gregory Nusinovich and Prof. Wes Lawson through useful discussions and important comments, during the course of this work.

References

[1] B. Richter, *1991 Part. Accel. Conf.* (San Francisco, CA, May 1991).
[2] V.L. Granatstein, P. Vitello, K.R. Chu, K. Ko, P.E. Latham, W. Lawson, C.D. Striffler and A. Drobot, *IEEE Trans. Nucl. Sci.*, **NS-32**, 2957 (1985).
[3] W. Lawson, J.P. Calame, B. Hogan, M. Skopec, C.D. Striffler and V.L. Granatstein, *IEEE Trans. on Plasma Science*, **20**, 216 (1992).
[4] S.G. Tantawi, W.T. Main, P.E. Latham, G.S. Nusinovich, W.G. Lawson, C.D. Striffler and V.L. Granatstein, *IEEE Trans. on Plasma Science*, **20**, 205 (1992).
[5] W. Lawson, H.W. Matthews, J.P. Calame, M.K.E. Lee, J. Cheng, B. Hogan, P.E. Latham, V.L. Granatstein and M. Reiser, *Phys. Rev. Lett.*, **71**, 456 (1993).
[6] G.P. Saraph, W. Lawson, M. Castle, J. Cheng, J.P. Calame and G.S. Nusinovich, *IEEE Trans. on Plasma Science*, **24**, 671 (1996).
[7] G.P. Saraph, V.L. Granatstein and W. Lawson, To be published in *IEEE Trans. on Electron Dev.*, **45**(4) (1998).
[8] J.M. Neilson, P.E. Latham, M. Caplan and W.G. Lawson, *IEEE Trans. Microwave Theory Tech.*, **37**, 1165 (1989).
[9] W. Lawson and P.E. Latham, *IEEE Trans. Microwave Theory Tech.*, **37**, 1165 (1989).
[10] P.E. Latham, W. Lawson and V. Irwin, *IEEE Trans. on Plasma Science*, **22**, 804 (1994).
[11] B. Levush and P.E. Latham, Private communication (1996).
[12] M.A. Moiseev and G.S. Nusinovich, *Radiophys. Quantum Electron.*, **17**, 1305, (1974).
[13] K.R. Chu, *Phys. Fluids*, **21**, 2354 (1978).
[14] B.G. Danly and R.J. Temkin, *Phys. Fluids*, **29**, 561 (1986).
[15] B. Levush and T.M. Antonsen, Jr., *IEEE Trans. on Plasma Science*, **18**, 260 (1990).
[16] G.P. Saraph, T.M. Antonsen, Jr., G.S. Nusinovich and B. Levush, *Phys. Fluids B*, **5**, 4473 (1993).
[17] W.B. Herrmannsfeldt, *SLAC Rep.* 226 (Stanford, CA, 1979).
[18] J. McAdoo, W.M. Bollen, A.H. McCurdy, V.L. Granatstein and R.K. Parker, *Int. J. Electron.*, **61**, 1025 (1986).
[19] G.S. Park, V.L. Granatstein, P.E. Latham, C.M. Armstrong, A.K. Ganguly and S.Y. Park, *IEEE Trans. on Plasma Science*, **19**, 632 (1991).
[20] M. Garven, B.G. Danly, M. Blank and M.J. Siegert, *22nd Int. Conf. on Infrared and Millimeter Waves*, p. 235 (Wintergreen, VA, July, 1997).
[21] G.S. Nusinovich and O. Dumbrajs, *Phys. of Plasmas* (1997).